JOURNAL GEOLOGICAL SOCIETY OF INDIA
Vol.86, November 2015, pp.513-518

Mineral Mapping of Lunar Highland Region using Moon Mineralogy Mapper (M^3) Hyperspectral Data

V. SIVAKUMAR[1*] and R. NEELAKANTAN[2]
[1]Department of Geology, Periyar University, Salem - 636 011, India
[2]Department of Industries and Earth Sciences, Tamil University, Tanjore - 613010, India
***Email:** v.sivakumars@gmail.com; [2]neels2004@gmail.com

Abstract: Mineral mapping of lunar surface is significant to understand the origin, crustal evolution, geological history and stratigraphy of the Moon. Advancements in orbital satellite sensor technology has allowed discriminating the minerals on lunar surface using hyperspectral data. The Moon Mineralogy Mapper (M^3) onboard Chandrayaan-1 provides unprecedented data of lunar surface to study about the Moon. In this paper, the minerals in and around Wegener crater on the lunar highland region was investigated using M^3 data. For this purpose, we used spectral similarity mapping (SSM) and band shape methods to discriminate minerals in this region. In SSM, dimensionality of M^3 data is reduced using Maximum Noise Fraction (MNF) and spectral end-members are extracted through Pixel Purity Index (PPI) algorithm. The mineralogical diversity is classified using Spectral Angle Mapper (SAM) algorithm. In addition, different band shape algorithms such as band curvature (bc), band strength (bs), band tilt (bt) and band ratio (br) at crucial wavelengths are applied to recognise the minerals. Low-Ca pyroxene (LCP) minerals are identified in and around this region. The presence of LCP minerals may be attributed to magmatic differentiation or later stage layered mafic intrusions.

Keywords: Chandrayaan-I, Highland, hyperspectral, low-Ca pyroxene, Moon, Moon Mineralogy Mapper, Wegener crater.

INTRODUCTION

Reflectance spectroscopic mapping method has been recognised as a useful technique for studying composition of the earth and planetary surface. Recent advancements in visible- to near- infrared orbital remote sensing has allowed spectral characterisation of minerals, thus assisting in lithological mapping based on mineralogy. Mineral mapping of lunar surface is important to understand the Moon's origin, evolution, geological diversity and history (e.g., Shuai et al., 2013; Jin et al., 2013). Many satellites (e.g., Galileo, Clementine) flown to Moon for various applications ranging from local to global scales, however, amount of information are limited due to spatial and spectral resolution constraints. Recently, hyper-spectral-imaging data from the M^3 onboard India's first Moon mission Chandrayaan-1 provided enormous data of lunar surface, which will be useful for new under-standing of the Moon (e.g., Moores et al., 2012; Borst et al., 2012).

In this study, mapping of minerals in and around Wegener crater on lunar highland region using M^3 data was attempted. The Moon is made up of a mixture of rocks of igneous character that largely varies both in chemistry and mineral composition which was discovered through Apollo program. The distinctions are between the lighter coloured feldspar-rich rocks of the highlands and the dark basalts of the maria (e.g., Vaniman et al., 1991). Compositionally, within the highland, rocks also have great diversity, such as ferroan anorthosites (rich Ca and Al), magnesium-rich and KREEP rocks (e.g., Heiken et al., 1991). Recent studies (e.g., Peterson et al., 1999; Anbazhagan and Arivazhagan, 2010) also suggested that highland region is predominantly composed of anorthositic rocks.

The highland surface has many impact craters than mare region, owing to the fact that surface is exposed to extensive impact activities; hence, the lunar highland surface is considered older than the mare surface (e.g., Ryder, 1990). The lunar highland samples (by Apollo 17) shows that some rocks have crystallised over 4.5 billion years ago, which is almost the age of the oldest meteorites (e.g., Christiansen and Hamblin, 1995). The isotopic ages of most highland rocks are around 3.9 to 4.0 billion years old (e.g., Christiansen and Hamblin, 1995).

Mineral Mapping

Moon minerals are distinguished in visible to near-infrared reflectance spectra by diagnostic absorption bands

due to transitions of electrons in the crystal field (e.g., Burns, 1993). The absorption graph shape, strength, and wavelength position of maximum absorption is controlled by the mineral's composition and crystal arrangement (e.g., Kramer, 2010). Recent studies (e.g., Anbazhagan and Arivazhagan, 2009; Anbazhagan and Arivazhagan, 2010; Klima et al., 2011; Chauhan et al., 2012; Pieters et al., 2013; Bharti et al., 2014) shows the potentials of spectroscopic mapping (hyperspectral imaging) for investigating the Moon mineral composition, lithology, etc.

Regional Setting

The study area is located in highland region (far side) of the Moon. This area was selected for this study because of its location coincides with the lunar highlands, where crustal thickness is very high (>30km) and topographically rugged terrain. The study area is located in higher latitude region and extends from approximately 113º W - 119º W; 42º N - 49º N (Fig. 1). The general elevation ranges approximately from -1000 m to 3000 m. Geologically this area is classified as Pre-Nectarian to Imbrian age (USGS, 1977) (Fig. 2).

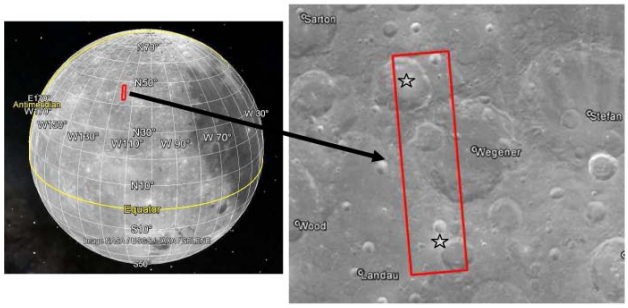

Fig.1. Study area location as shown in red colour box on the image captured from google moon tool (2014). Star mark indicates the fresh exposures (appearing brighter) .

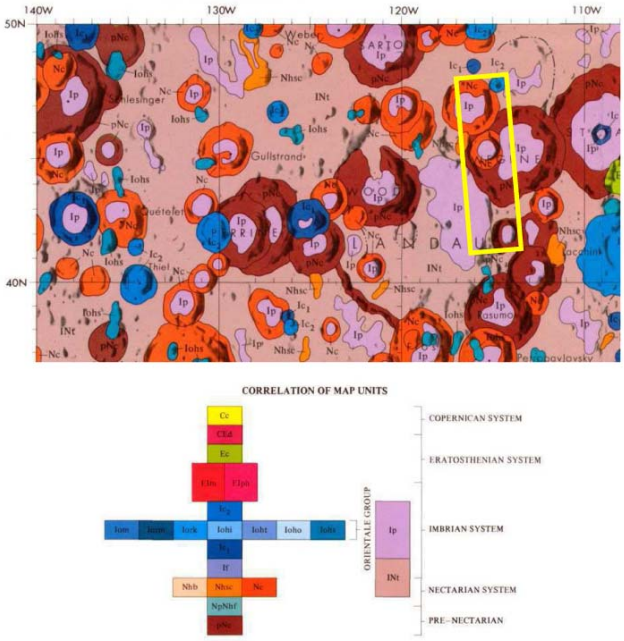

Fig.2. Yellow colour box shows extent of study area on geology map. Cc-crater material, Ip-Plains material, Iohs-Secondary crater facies, Ic_1 / Ic_2 – crater material, INt-Terra material, Nhsc-Hertzsprung secondary crater material, Nc- crater material, pNc - crater material. Geological atlas of the moon – west side of the moon (I-1034) downloaded from http://www.lpi.usra.edu/resources/mapcatalog/usgs/.

MATERIALS AND METHOD

The M^3 data was used for mapping the minerals in and around Wegener crater. The M^3 sensor was a guest instrument from NASA on the Chandrayaan-1, the Indian Space Research Organisation's (ISRO) first mission to the Moon (Goswami and Annadurai, 2009). The sensor records the reflected radiance from the Moon's surface in pushbroom mode between 0.46 and 2.97 μm in 85 contiguous spectral bands and 20 – 40 nm spectral sampling with 140 – 280 m spatial resolution (Pieters et al., 2009). Photometrically and thermally corrected Level-2 data was downloaded from Planetary Data System (PDS) geosciences node (http://ode.rsl.wustl.edu/Moon/) for this study.

Environment for Visualising Images (ENVI) software was used for data processing, analysing and mapping minerals. An image subset representing the study region from the M^3 data was clipped from the orbital coverage (M3G20090118T022705_V01_RFL) (Fig. 3a). The hypercube data was corrected for the coherent and non-coherent noises and also for high-dimensionality using Maximum Noise Fraction (MNF) method, which is commonly used for reducing dimensionality in hyperspectral remote sensing data (e.g., Wang and Chang, 2006). MNF output was used for identifying the compositionally unique end-member spectra. The Pixel Purity Index (PPI) algorithm (e.g., Boardman, 1994) was used to categorise the spectrally distinctive end-member spectra. End-members were plotted in ENVI plot window and continuum was removed for all end-member spectras for better understanding of absorption parameters. Spectras are exported to ASCII format to analyse for spectral charaterstics such as peak absorptions, strength of absorption and Full width at half maximum (FWHM) for understading mineral wealth across the spectrum. OriginPro version 8.0 software was used to analyse spectral charaterstics.

The Spectral Angle Mapper (SAM) algorithm (Kruse et al., 1993) was used for identifying spatial distribution of

mineral categories in the study area. SAM classifies the pixels based on the similarity between the reference end-members and unknown pixel spectra. It calculates the angle between target spectra and reference end-member spectra and subsequently assigns the target pixels to a certain class based on the weights (thresholds) between 1 (perfect match) and 0 (no match) (e.g., Dennison et al., 2004). SAM technique is not affected by solar illumination causes, as angle between two vectors is self-determining of the vectors length (e.g., Crosta et al., 1998; Kruse et al., 1993). SAM algorithm is given below (Kruse et al., 1993; Van der Meer et al., 1997):

$$\alpha = \cos^{-1}\left[\frac{\sum_{i=1}^{nb} t_i r_i}{\left(\sum_{i=1}^{nb} t_i^2\right)^{\frac{1}{2}}\left(\sum_{i=1}^{nb} r_i^2\right)^{\frac{1}{2}}}\right]$$

where, nb is the number of bands, t_i is the target spectrum (pixel), and r_i is the reference spectra.

In addition to SAM method, we adopted band shape algorithms such as band strength (bs), band curvature (bc), band tilt (bt) and band ratio (br) at crucial wavelengths to delineate such as olivine, low-Ca pyroxene, high-Ca pyroxene and anorthosite. These approaches are appropriate to distinguish the particular minerals in a false colour composite map (e.g., Borst et al., 2012). Above techniques are used for Clementine UV/VIS and NIR data by (Borst et al., 2012). We extended their comprehensive methods to M^3 data to discriminate specific minerals on lunar surface. These methods facilitates to analyse the results obtained from SAM (e.g., Isaacson et al. 2011). The band strength (bs), band curvature (bc), band tilt (bt) and band ratio (br) at appropriate wavelengths were calculated from ratio 1μm/ 0.75 μm, 0.75 μm /1 μm + 1 μm /0.9 μm, 1 μm /1 μm and 2 μm /1.25 μm, respectively. A summary of the band ratio techniques used in this study is presented in Table 1.

Table 1. A summary of the band ratio techniques, adopted from Borst et al. (2012)

Parameters	Visible			NIR
	Band Strength	Band Curvature	Band Tilt	Olivine/ Pyroxene
Colour	Blue	Red	Green	Black/ White
Wavelength ratio (μm)	1/0.75	0.75/0.9+1/0.9	0.9/1	2/1.25
Olivine	Low	Medium+Low	Highest	Highest
Low-Ca pyroxene	Medium	High+Highest	Lowest	Medium
High-Ca pyroxene	Low	High+Low	Medium	Lowest
Anorthosite	High	Lowest+Low	Low	Low

RESULTS AND DISCUSSION

Figure 3b shows the output of SAM classified image. Total seven image end-members were processed through SAM algorithm and good distinction was found. The mineralogical variations have been observed within the fresh (appearing bright) craters and crater rim region (Fig. 3b). Fresh (bright) craters (star marking in Fig. 1) shows good variation in mineralogy.

Figure 4 shows the different end-member spectras (EMS) of M^3 data. EMS absorption characteristics are shown in Table 2. EMS 1,2, and 7 shows relatively stronger and

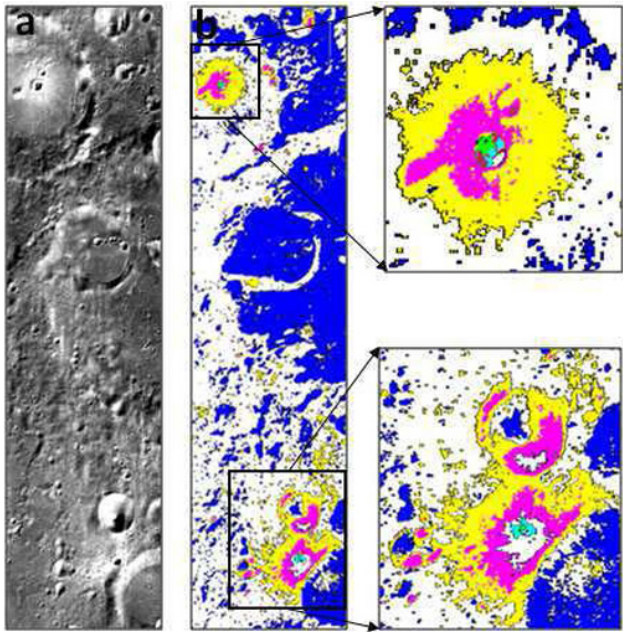

Fig.3. Shows result of SAM classification. **(a)** Left panel showing the M3 image of the study area. **(b)** Black colour boxes highlight the areas where maximum mineralogical diversity is present in the study area.

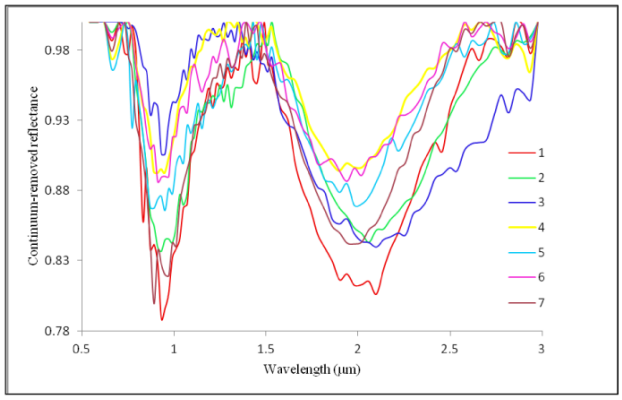

Fig.4. End-member spectra derived from image shows different minerals. Total seven end-members (1-7) are derived from n-D visuvaliser. EMS 1 – 7 shown in different colour in graph and presented in simliar colour code in Fig. 3.

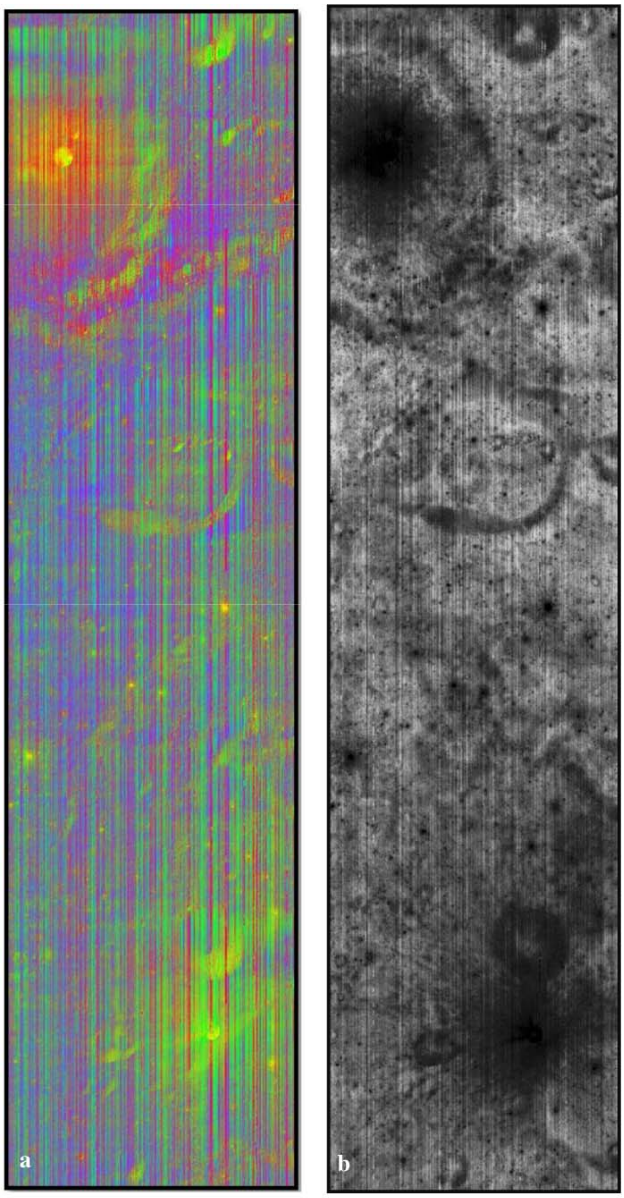

Fig.5. (a) RGB of the three integrated band depths (Blue: 1 μm / 0.75 μm, Red: 0.75 μm /0.9 μm + 1 μm /0.9 μm, Green: 0.9 μm /1 μm). In RGB composite, blue colour indicates anothositic/weathered rocks. Red - pink colour shows LCP (pyroxene with high Fe/Mg). Green - yellow colour indicates LCP with modest of Fe/Mg. **(b)** Grayscale image shows the ratio of 2 μm /1.25 μm. The probable olivine-dominated rock (mafic composition) areas indicate high value (high intensity / brighter view in the image. Low value (low intensity) shows possible LCP-dominated rocks.

narrow absortions (narrow absorption inferred through FWHM) near 1 μm and broad absorption near 2 μm wavelength regions. Decreasing amount of absorptions are observed for EMS 5, 6, 4, 3 and 5, 6, 3, 4 in same order near 1 μm and 2 μm regions, respectively. This spectral absorption indicates the presence of LCP mineral. The Moon LCP mineral spectral characteristics are well documented to distinguish through visible and NIR spectroscopic measurements (e.g., Adams, 1974; Sunshine and Pieters, 1993; Klima et al., 2008; Klima et al., 2011). The varying amount of absorptions strength near 1 μm due to contribution of Mg and Fe content in pyroxene crystallographic sites. Generally, strong absorption towards shorter wavelength area denotes the modest amounts of a ferric oxide mixture with pyroxenes (e.g., Adams, 1974). EMS 1 and 2 shows 2 μm absorption band shifts towards longer wavelenght region (Fig. 4 and Table 2). This is probably due to contribution of Ca^{+} in pyroxene structure (near 2 μm) or thermal history of pyroxene (e.g., Klima et al., 2008). EMS 3 shows significantly weaker absorption near 1 μm then 2 μm (Fig. 4 and Table 2), which may be due to the presence of possible Fe-Mg-spinel lithology on the surface (e.g., Pieters et al., 2014; Pathak et al., 2015).

Figure 5a shows composite of various band ratios such as bs, bc, bt and br at crucial wavelengths. Those were calculated from ratio between 1μm/0.75 μm, 0.75 μm/1 μm + 1 μm /0.9 μm, 1 μm /1 μm and 2 μm /1.25 μm, respectively. The bt, br and bs ratio outputs were displayed in RGB composite, respectively (Fig. 5a). The bs values are high (blue colour), which indicates probable anorthositic/ weathered rocks. Generally, weathered soils shows high bs values as result of space weathering (e.g., Tompkins et al., 1997). The bc indicates presence of LCP (pyroxene with high Fe/Mg) in the lunar surface, which is appearing in red - pink colour in RGB composite (Fig. 5a). Higher band tilt value indicates (Green - yellow colour) LCP with

Table 2. Absorption characteristics of end-member spectras

End-member (EMS)	Absorption region (μm)	Wavelength of Peak Absorption (μm)	Absorption Strength Ratio	FWHM
1	1	0.930	0.119	0.257
	2	2.098	0.105	0.654
2	1	0.930	0.075	0.233
	2	2.058	0.076	0.619
3	1	0.930	0.051	0.153
	2	2.098	0.061	0.676
4	1	0.950	0.051	0.164
	2	1.898	0.059	0.559
5	1	0.950	0.059	0.225
	2	1.978	0.065	0.577
6	1	0.910	0.052	0.178
	2	1.938	0.061	0.643
7	1	0.890	0.083	0.176
	2	2.018	0.083	0.597

modest of Fe/Mg. The possible olivine and LCP rich areas were delineated through ratio of 2 μm /1.25 μm (Fig.5b). The high and low ratio values suggest the presences of olivine (likely) and LCP dominated rocks, respectively. The mafic intrusive rocks appear bright in grayscale image (e.g., Borst et al., 2012) (Fig. 5b). The identified LCP mineral exposure corresponds to Imbrian age units (Ip), which is represented on the geologic map of the region (USGS, 1977).

The possibilities of LCP origin on lunar highland surface based on M^3 data are: (A) A possible hypothesis for origin of LCP may be the uppermost lunar Magma Ocean cumulates (e.g., Hess and Parmentier, 1995) could be well mixed or removed due to consecutive impact events or weathered. Thus, most mafic minerals are remnant on the surface. (B) The layered early intrusive plutons are common on the lunar surface (e.g., Raedeke and McCallum, 1980) and also the hemical compositions of minerals varies according to their crystallisation order and thermal history as mafic intrusive material approaching the surface (e.g., Cahill et al., 2009). Therefore, exposure of plutons is a possible hypothesis for the origin of LCP minerals.

CONCLUSION

Using M^3 hyperspectral data form Chandrayaan-1, spectrally dominant LCP minerals have been identified in and around Wegener crater on lunar highland region. The SSM method and band shape methods are helpful to discriminate mineralogy in Visble-NIR reflectance spectra. LCP and minerals were identified from M^3 data using SSM and band shape parameter approaches. The identified LCP mineral exposure corresponds to Imbrian age units (Ip). The presence of LCP with diverse spectral absorption characteristics may be attributed to magmatic differentiation or later stage layered mafic intrusion in the Moon. Further, this study suggests that fresh (bright) exposures (very recent impact) are good candidate for mapping the bedrock geology. Future work would focus on examining compositional trends at different regions of the Moon and analysing ages of the rocks to determine the origin, occurrence and distribution.

Acknowledgement: We wish to acknowledge M^3 (Level-2 data) and LOC team for supplying the data through Geoscience PDS Node. We would like to take this opportunity to thank the Editor and the anonymous reviewers for their valuable comments and suggestions, which have been helpful in order to enhance the technical content and presentation of the manuscript. Currently first author is working with C-DAC, Pune, India. First author thankfully acknowledges C-DAC for providing resources and support to carry out the study.

References

Adams, J.B. (1974) Visible and near-infrared diffuse reflectance spectra of pyroxenes as applied to remote sensing of solid objects in the solar system. Jour. Geophys. Res., v.79, no.32, pp.4829-4835.

Anbazhagan, S. and Arivazhagan, S. (2009) Reflectance spectra of analog basalts; implications for remote sensing of lunar geology. Planet. Space Sci., v.57, no.12, pp.1346-1358.

Anbazhagan, S. and Arivazhagan, S. (2010) Reflectance spectra of analog anorthosites: Implications for lunar highland mapping. Planet. Space Sci., v.58, no.5, pp.752-760.

Bharti, R., Ramakrishnan, D. and Singh, K.D. (2014) Compositional diversity of near-, far-side transitory zone around Naonobu, Webb and Sinus Successus craters: Inferences from Chandrayaan-1 Moon Mineralogy Mapper (M3) data. Jour. Earth System Sci., v.123, no.1, pp.233-246.

Boardman, J.W. (1994). Geometric mixture analysis of imaging spectrometery data, Proc. Int. Geoscience and Remote Sensing Symp., v.4, pp. 2369-2371.

Borst, A.M., Foing, B.H., Davies, G.R. and Van Westrenen, W. (2012). Surface mineralogy and stratigraphy of the lunar South Pole-Aitken basin determined from Clementine UV/VIS and NIR data. Planetary and Space Science, v.68, no.1, pp.76-85.

Burns, R.G. (1993). Mineralogical applications of crystal field theory. Cambridge Univ. Press., v.5, pp.220-242.

Christiansen, E.H. and Hamblin, K.W. (1995) Exploring the planets, chapter-4, 2nd Edition, Prentice Hall, ISBN 0-02-322421-5, v.1, pp.xi-500.

Cahill, J.T.S., Lucey, P.G. and Wieczorek, M.A. (2009) Compositional variations of the lunar crust: Results from radiative transfer modeling of central peak spectra. Jour.Geophys. Res., v.114, no. E09001, doi:10.1029/2008JE003282.

Crosta, A.P., Sabine, C. and Taranik, J.V. (1998) Hydrothermal Alteration Mapping at Bodie, California, using AVIRIS Hyperspectral Data.Remote Sensing of Environment, v. 65, pp.309-319

Dennison, P.E., Halligan, K.Q. and Roberts, D.A. (2004) A comparison of error metrics and constraints for multiple end-member spectral mixture analysis and spectral angle mapper, Remote Sens. Environ., v.93, no.3, pp. 359-367.

Chauhan, P., Kaur, P., Srivastava, N., Bhattacharya, S., Kumar, A.S. and Goswami, J.N. (2012) Compositional and morphological analysis of high resolution remote sensing data

over central peak of Tycho crater on the Moon: implications for understanding lunar interior. Curr. Sci., v.102, no.7, pp.1041-1046.

Goswami, J.N. and Annadurai, M. (2009) Chandrayaan-1: India's first planetary science mission to the Moon, Lunar Planetary Science (CDROM), Abstract, v.40, pp.2571.

Heiken, G., Vaniman, D. and French, B.M. (Eds.) (1991) Lunar sourcebook: A user's guide to the Moon. CUP Archive, pp.595-632.

Hess, P.C. and Parmentier, E.M. (1995) A model for the thermal and chemical evolution of the Moon's interior: Implications for the onset of mare volcanism. Earth Planet. Sci. Lett., v.134, no.3, pp.501-514.

Jin, S., Arivazhagan, S. and Araki, H. (2013) New results and questions of lunar exploration from SELENE, Chang'E-1, Chandrayaan-1 and LRO/LCROSS. Adv. Space Res., v.52, no.2, pp.285-305.

Isaacson, Peter J., Carle M. Pieters, Sebastien Besse, Roger N. Clark, James W. Head, Rachel L. Klima, John F. Mustard, et al. (2011) Remote compositional analysis of lunar olivine rich lithologies with Moon Mineralogy Mapper (M3) spectra. Jour. Geophys. Res. Planets (1991–2012), v.116, no. E6.

Klima, R.L., Pieters, C.M. and Dyar, M.D. (2008) Characterisation of the 1.2 ìm M1 pyroxene band: Extracting cooling history from near-IR spectra of pyroxenes and pyroxene dominated rocks. Meteoritics Planet Sci, v.43, no.10, pp.1591-1604.

Klima, Rachel L., Carle M. Pieters, Joseph W. Boardman, Robert O. Green, James W. Head, Peter J. Isaacson, John F. Mustard, et al. (2011) New insights into lunar petrology: Distribution and composition of prominent low-Ca pyroxene exposures as observed by the Moon Mineralogy Mapper (M^3). Jour. Geophys Res. Planets (1991–2012), v.116, no. E6.

Kramer, G.Y. (2010) Characterizing bedrock lithologies using small crater rim and ejecta probing (SCREP). Adv. Space Res., v.45, no.10, pp.1257-1267.

Kruse, F.A., Lefkoff, A.B., Boardman, J.B., Heidebrecht, K.B., Shapiro, A.T., Barloon, P.J. and Goetz, A. F. H. (1993) The Spectral Image Processing System (SIPS) - Interactive Visualisation and Analysis of Imaging spectrometer Data. Remote Sensing Environ., v.44, pp.145-163.

Moores, John E., Raymond Francis, Marianne Mader, G., Osinski, R., Barfoot, T., Barry, N., Basic G., et al. (2012) A Mission Control Architecture for robotic lunar sample return as field tested in an analogue deployment to the sudbury impact structure. Adv. Space Res., v.50, no.12, pp.1666-1686.

Pathak, S., Singh, R., Chauhan, M., Bhattacharya, S. and Chauhan, P. (2015) Remote observation of lunar crater Hayn for mineralogical analysis using datasets from recent lunar missions, European Planetary Science Congress 2015, EPSC Abstracts, v.10, pp.EPSC2015-559.

Peterson, C.A., Hawke, B.R., Lucey, P.G., Taylor, G.J., Blewett, D.T. and Spudis, P.D. (1999) The Distribution of Anorthosite on the Lunar Farside. *In* New Views of the Moon 2: Understanding the Moon Through the Integration of Diverse Datasets, v.1, pp.46.

Pieters, C.M., Hanna, K.D., Cheek, L., Dhingra, D., Pprissel, T., Jackson, C. and Taylor, L. A. (2014) The Second Conference on the Lunar Highlands Crust and New Directions, The distribution of Mg-spinel across the Moon and constraints on crustal origin, American Mineralogist, v.99(10), pp.1893-1910.

Pieters, C.M., Donaldson Hanna, K., Cheek, L., Dhingra, D., Moriarty, D., Parman, S. and Prissel, T. (2013) Compositional Evolution of the Early Lunar Crust: Observed Diverse Mineralogy of the Upper and Lower Crust. Lunar Planetary Sci. Contrib., no.1719, pp.2545.

Pieters, C.M., Goswami, J.N., Clark, R.N., Annadurai, M., Boardman, J.,. Buratti, B., Combe, J.P., et al. (2009) Character and spatial distribution of OH/H2O on the surface of the Moon seen by M3 on Chandrayaan-1. Science, v.326, no.5952, pp.568-572.

Raedeke, L.D. and McCallum, I.S. (1980) A comparison of fractionation trends in the lunar crust and the Stillwater complex. *In:* R.B. Merrill and J.J. Papike Pergamon (Eds.) Lunar Highlands Crust. New York, pp.133-153.

Ryder, G. (1990) Lunar samples, lunar accretion and the early bombardment of the Moon. EoS, Trans. Amer. Geophys. Union, v.71, no.10, pp.313-323.

Shuai, T., Zhang, X., Zhang, L. and Wang, J. (2013) Mapping global lunar abundance of plagioclase, clinopyroxene and olivine with Interference Imaging Spectrometer hyperspectral data considering space weathering effect. Icarus, v.222, no.1, pp.401-410.

Sunshine, J.M. and Pieters, C.M. (1993) Estimating modal abundances from the spectra of natural and laboratory pyroxene mixtures using the modified Gaussian model. Jour. Geophys. Res., Planets (1991–2012), v.98, no.E5, pp.9075-9087.

Tompkins, S., Mustard, J.F., Pieters, C.M. and Forsyth, D.W. (1997) Optimisation of end-members for spectral mixture analysis. Remote Sensing Environ., v.59, pp.472–489.

USGS (1977) Geological atlas of the Moon – west side of the Moon (I-1034), USGS.

Van Der Meer, F., Vasquez-Torres, M. and Van Dijk, P.M. (1997) Spectral Characterisation of Ophiolite Lithologies in the Troodos Ophiolite Complex of Cyprus and its Potential in Prospecting for Massive Sulphide Deposits. Internat. Jour. Remote Sensing, v.18, no.6, pp.1245-1257.

Vaniman, D., Dietrich, J., Taylor, G.J. and Heiken, G. (1991) Exploration, samples, and recent concepts of the Moon. Lunar Sourcebook, pp.5-26.

Wang, J. and Chang, C.I. (2006) Independent component analysis-based dimensionality reduction with applications in hyperspectral image analysis; IEEE Trans. Geosci.Remote Sens., v.44, no.6, pp.1586-1600.

(Received: 14 June 2014; Revised form accepted: 12 January 2015)